Structural flexibility at a major conserved antibody target on hepatitis C virus E2 antigen

Leopold Kong[a,1], David E. Lee[b], Rameshwar U. Kadam[a], Tong Liu[b], Erick Giang[c], Travis Nieusma[a], Fernando Garces[a], Netanel Tzarum[a], Virgil L. Woods Jr.[b,2], Andrew B. Ward[a], Sheng Li[b], Ian A. Wilson[a,d,3], and Mansun Law[c,3]

[a]Department of Integrative Structural and Computational Biology, The Scripps Research Institute, La Jolla, CA 92037; [b]Department of Medicine, University of California, San Diego, La Jolla, CA 92037; [c]Department of Immunology and Microbial Science, The Scripps Research Institute, La Jolla, CA 92037; and [d]The Skaggs Institute for Chemical Biology, The Scripps Research Institute, La Jolla, CA 92037

Edited by Peter Palese, Icahn School of Medicine at Mount Sinai, New York, NY, and approved September 6, 2016 (received for review June 16, 2016)

Hepatitis C virus (HCV) is a major cause of liver disease, affecting over 2% of the world's population. The HCV envelope glycoproteins E1 and E2 mediate viral entry, with E2 being the main target of neutralizing antibody responses. Structural investigations of E2 have produced templates for vaccine design, including the conserved CD81 receptor-binding site (CD81bs) that is a key target of broadly neutralizing antibodies (bNAbs). Unfortunately, immunization with recombinant E2 and E1E2 rarely elicits sufficient levels of bNAbs for protection. To understand the challenges for eliciting bNAb responses against the CD81bs, we investigated the E2 CD81bs by electron microscopy (EM), hydrogen–deuterium exchange (HDX), molecular dynamics (MD), and calorimetry. By EM, we observed that HCV1, a bNAb recognizing the N-terminal region of the CD81bs, bound a soluble E2 core construct from multiple angles of approach, suggesting components of the CD81bs are flexible. HDX of multiple E2 constructs consistently indicated the entire CD81bs was flexible relative to the rest of the E2 protein, which was further confirmed by MD simulations. However, E2 has a high melting temperature of 84.8 °C, which is more akin to proteins from thermophilic organisms. Thus, recombinant E2 is a highly stable protein overall, but with an exceptionally flexible CD81bs. Such flexibility may promote induction of nonneutralizing antibodies over bNAbs to E2 CD81bs, underscoring the necessity of rigidifying this antigenic region as a target for rational vaccine design.

hepatitis C virus | E2 | CD81-binding site | conformational flexibility | protein dynamics

Hepatitis C virus (HCV) is a leading cause of liver cirrhosis and hepatocellular carcinoma, infecting more than 2% of the world's population (1). HCV infection is highly prevalent in developing countries and among marginalized populations, such as injection drug users (IDUs) and prisoners in developed countries (2). Effective direct-acting antiviral (DAA) drugs have been developed recently to curb the advance of HCV (3, 4). Nevertheless, new infections are on the rise among young IDUs in developed countries and along drug-trafficking routes (2, 5, 6). Because DAA treatment is prohibitively expensive and does not prevent reinfection (7, 8), an effective vaccine is essential for management of the global HCV epidemic (9–11).

Despite the significant public health burden, no effective prophylactic vaccine against HCV has been developed. High genetic variability of the virus is a major barrier, particularly in the E1 and E2 envelope glycoproteins that are the primary neutralizing antibody (NAb) targets. E2, the receptor-binding protein, mediates cell entry by interacting with the tetraspanin CD81 and several other cell surface molecules (12, 13). The crystal structure of the E2 core domain (E2c) consists of a central β-sandwich flanked by "front" and "back" layers (14) (Fig. 1). The CD81-binding site (CD81bs) has been mapped by mutagenesis and electron microscopy (EM) to various elements: a conserved N-terminal region (residues 412–423), the front layer (residues 424–453), and the adjacent CD81-binding loop (CD81bl; residues 519–535) (14–16) (Fig. 1). The CD81bs is also a conserved antigenic site recognized by multiple broadly neutralizing antibodies (bNAbs) and, therefore, an important target for HCV vaccine design. So far, three distinct clusters of neutralizing epitopes, or antigenic sites, have been identified within the CD81bs. The first antigenic site (AS412) consists of the conserved N-terminal end of the CD81bs spanning residues 412–423. The bNAbs AP33, HCV1, HC33.1, and 3/11 primarily bind to E2 at AS412, and their interactions have been structurally characterized (17–22). The second antigenic site (AS434) consists of a short α-helix in the front layer residues 434–446. The bNAbs HC84-1 and HC84-27 and the weakly neutralizing monoclonal antibody (mAb) 8 primarily recognize this helical region (23, 24). The third cluster of neutralizing epitopes that we call antigenic region 3 (AR3) is a discontinuous surface composed of the entire front layer, including AS434, and the adjacent CD81bl. AR3 is recognized by a family of potent bNAbs consisting of AR3A, AR3B, AR3C, and AR3D (25, 26).

There is ample evidence that the E2 CD81bs is accessible and immunogenic on the virion and on recombinant E2. First, the CD81bs is recognized by bNAbs with different angles of approach (9) (Fig. S1). Second, although E2 is densely glycosylated,

Significance

Hepatitis C virus is an important human pathogen, and its E2 envelope glycoprotein is the major target of neutralizing antibodies (NAbs) and, hence, a promising vaccine candidate. Many broadly NAbs (bNAbs) to E2 recognize the conserved receptor-binding site, but immunization with soluble E2 antigen rarely elicits a potent bNAb response. Here, we show that soluble E2 is highly stable except for the receptor-binding site and variable loops. Thus, despite high sequence conservation, structural flexibility at the receptor-binding site may distract the immune system from eliciting bNAbs that recognize the conformation required for its function on virions. Stabilization of the E2 CD81 receptor-binding site (CD81bs) by structure-based design may improve its performance as a vaccine candidate.

Author contributions: L.K., V.L.W., I.A.W., and M.L. designed research; L.K., D.E.L., R.U.K., T.L., E.G., T.N., F.G., and N.T. performed research; L.K., R.U.K., A.B.W., and S.L. analyzed data; and L.K., I.A.W., and M.L. wrote the paper.

The authors declare no conflict of interest.

This article is a PNAS Direct Submission.

Data deposition: The electron microscopy reconstruction of the complex consisting of hepatitis C virus (HCV) E2 core domain bound to antigen-binding fragments antigenic region 1B (AR1B), AR2A, and HCV1 has been deposited with the Electron Microscopy Data Bank under accession codes EMD-8338, EMD-8339, and EMD-9340.

[1]Present address: Structural Cell Biology Section, Laboratory of Cell and Molecular Biology, National Institute of Diabetes and Digestive and Kidney Diseases, National Institutes of Health, Bethesda, MD 20814.

[2]Deceased September 30, 2012.

[3]To whom correspondence may be addressed. Email: mlaw@scripps.edu or wilson@scripps.edu.

This article contains supporting information online at www.pnas.org/lookup/suppl/doi:10.1073/pnas.1609780113/-/DCSupplemental.

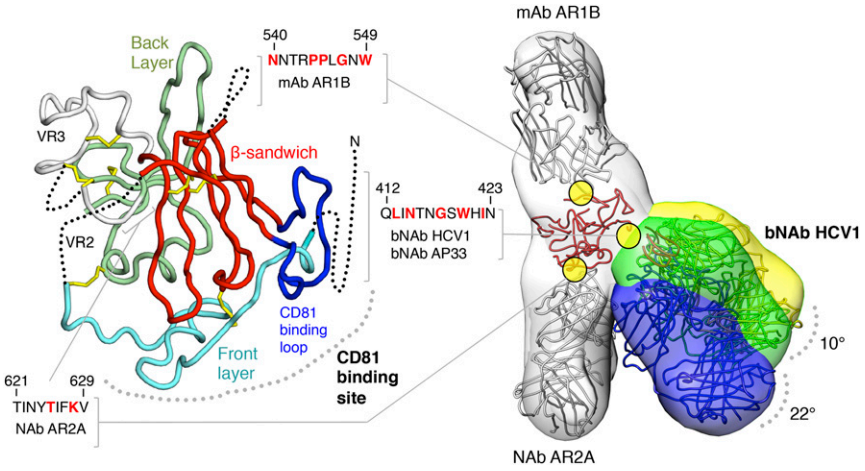

Fig. 1. Conformational flexibility of a broadly neutralizing epitope on soluble HCV E2c2 revealed by EM. (*Left*) Crystal structure of E2c is displayed as a ribbon with structural elements indicated and disordered regions shown as dotted lines. The epitopes of mAb AR1B, bNAb HCV1, bNAb AP33, and NAb AR2A are defined; residues that are important for binding, as mapped by alanine scanning experiments, are colored red in the sequences shown. (*Right*) Three negative-stain EM density maps at ~30-Å resolution of E2c2 (gray) bound to Fab AR1B (gray), AR2A (gray), and HCV1 (yellow, green, and blue) are shown as transparent surfaces with structural models of the antibodies and E2c superimposed (also Fig. S3). Differences in bNAb HCV1 angles of approach indicated from the three RCT reconstructions are shown.

the CD81bs is not obstructed by any of the 11 *N*-linked glycans (14). Third, antibody responses to the CD81bs are frequently detected in sera from subjects immunized with the candidate vaccine immunogens: soluble E2 or E1E2. However, these serum antibodies are often weak or nonneutralizing despite high anti-E1E2 antibody titers (14, 27–30). Indeed, mAbs have been isolated to the different components of the CD81bs, but only a few (mentioned above) cross-neutralize the highly diverse HCV genotypes (30–33). In a panel of 37 mAbs isolated from mice immunized with E1E2, 20 (54%) and four (11%) bind to the E2 front layer and CD81bl, respectively, but none neutralize HCV (30). The results indicate that the E2 front layer and CD81bl are highly immunogenic but likely contain structural features that act as decoys for the immune system, skewing the response to nonneutralizing epitopes during immunization. Interestingly, in the antibody panel, of seven mAbs that bind subsite AS412, six are neutralizing, suggesting at least that AS412 is presented correctly; however, sufficient levels of NAbs were not produced in the animals. Thus, to understand how to elicit bNAbs to the E2 CD81bs, it is necessary to investigate anti-CD81bs antibodies and the E2 antigens in depth.

In this study, we first investigated the molecular features of the E2 CD81bs. We used EM to elucidate the interactions between E2 and a bNAb targeting AS412. Next, we mapped the surface accessibility and flexibility of E2 through hydrogen–deuterium exchange mass spectrometry (HDXMS). The HDX results were then corroborated by molecular dynamics (MD) simulations using available crystal structures. To assess the overall stability of E2, we used differential scanning calorimetry (DSC) and determined binding entropies of various E2 ligands using isothermal titration calorimetry (ITC). The combined results suggest recombinant E2 is a highly stable protein with an exceptionally flexible receptor-binding site that can present many nonoptimal conformations/configurations during immunization. Furthermore, we can now use this information to guide engineering efforts to stabilize the E2 CD81bs to advance HCV vaccine design.

Results and Discussion

Flexibility at the E2 CD81bs as Visualized by EM. The first structural investigations of HCV E2 revealed that AS412 within the E2 CD81bs, when presented as a synthetic peptide, forms a β-hairpin when bound to bNAbs HCV1 and AP33 (17–20). Both HCV1 and AP33 interact with one face of the AS412 β-hairpin, whereas the opposite face contains an *N*-linked glycan. These initial results suggest that both faces of the AS412 β-hairpin are solvent-accessible and that AS412 might protrude from the E2 protein as a potentially flexible, flap-like structure (18). Interestingly, AS412 is disordered in the published HCV E2c crystal structure (14). Furthermore, recent structures of the AS412 peptide in complex with bNAbs HC33.1 and 3/11 revealed very different, extended conformations for the peptide (21, 22).

To investigate the flexibility of AS412 in the context of E2, we sought to visualize directly any structural heterogeneity in the interaction between bNAb HCV1 and an E2c variant (E2c2; the amino acid sequence of E2c variants are shown in Fig. S2) containing a full variable region 2 (VR2) (Fig. 1 and Fig. S3). Assuming that HCV1 primarily interacts with E2 via AS412, flexibility at AS412 should translate to larger, rigid-body motions for HCV1, as previously observed for anti–HIV-1 bNAb PG9 when bound to HIV-1 envelope glycoprotein gp120 as a monomer (34). Therefore, we formed a complex composed of partially deglycosylated E2c2 bound to the antigen-binding fragments (Fabs) of mAb AR2A, mAb AR1B, and bNAb HCV1, and performed reference-free alignment and classification. Previously, we showed by mutagenesis or negative-stain EM that attachment of AR2A or AR1B to E2 did not significantly alter binding of CD81 or mAb AR3C (14). AR2A and AR1B were incorporated into the complex as fiduciary markers to help orient the E2 structure. Interestingly, substantial heterogeneity was observed at one protrusion in the 2D classes that corresponded to a single Fab. Because of this heterogeneity, we collected random conical tilt (RCT) EM data of the complex and calculated multiple 3D reconstructions (Fig. 1 and Fig. S3). Altogether, the 2D classes were consistent with three separate 3D reconstructions, each containing three protrusions of density corresponding to each of the three Fabs used to construct the complex, with E2c2 at the center. As expected from the 2D classes, there was substantial structural variation for one of the Fabs. To assign identities to each EM density protrusion, we relied on a previous mapping study (25), an alanine scanning experiment (Table S1), the E2c/AR3C Fab complex crystal structure (14), and the E2c-AR2A-CD81 EM structure (14). In this manner, we were able to assign AR2A and AR1B unambiguously to protrusions in the reconstruction that extend in opposite directions from each other. The third EM protrusion was consistent with the location of AS412 on E2 based on the AR1B and AR2A assignments. We therefore identified this more variable protrusion as the HCV1 Fab. Remarkably, the HCV1 Fab exhibited 10–22° variation in the angle of approach between the three 3D reconstructions (Fig. 1). Compared with the nearly 180° variation observed for anti-HIV1 bNAb PG9 when bound to HIV-1 gp120 monomer, the flexibility of HCV1 is modest. However, PG9 recognizes the V1V2 loop, which is 57–80 residues and highly flexible in the context of gp120 monomer, whereas HCV1 recognizes AS412, which is merely 12 residues and only five residues from the first disulfide bond to the core of the E2 protein. Thus, the observed variability

of HCV1 is consistent with the originally proposed hypothesis that AS412 is a flap-like structure with structural flexibility, but somewhat constrained by the close proximity to the rest of the E2 protein (18). Of note, the negative-stain EM results are not of sufficient resolution to elucidate whether small, local conformational changes could occur in the E2 front layer and/or CD81bl in the antibody-bound E2.

Mapping the Conformational Flexibility of HCV E2 by HDX. Next, we sought to extend our investigation on flexibility to the rest of the E2 protein using HDX. HDX tracks the rate of deuterium incorporation into the backbone amides of proteins when exposed to deuterated solvent, and is highly dependent on the conformational flexibility and accessibility of individual residues in the protein (35). Here, we used HDXMS to measure the masses of enzymatically cleaved peptides from E2 after E2 had been exposed to deuterated solvent over different lengths of time and then quenched to stop the exchange (36). In this manner, three complexes were analyzed with HDX: partially deglycosylated E2c2 bound to Fab AR2A (E2c2-AR2A), partially deglycosylated E2c2 bound to Fabs AR2A and AP33 (E2c2-AR2A-AP33), and partially deglycosylated full-length E2 ectodomain (E2ΔTM) bound to Fabs AR2A and AP33 (E2ΔTM-AR2A-AP33). The E2 proteins were enzymatically deglycosylated with endoglycosidase H (EndoH) to maximize the identification of peptides and the overall peptide coverage of the proteins. Fab AR2A, which does not bind to the CD81bs, was required in the deglycosylation step to prevent E2 aggregation and ensure complete protease digestion.

Multiple peptic fragments of the complexes were identified by MS, covering 85% of E2c2 and 60% of E2ΔTM (Figs. S4 and S5). Considering the relatively small size of E2 in relation to its relatively large proportion of prolines that are inaccessible by HDX (25 of 335 E2ΔTM residues are prolines), the variable glycosylation states of the proteins, and the low yield of glycopeptides identifiable in MS, the HDX coverage achieved in this study is on par with a previous HDX study of Ebola virus envelope glycoprotein (37). To facilitate analysis, we focused on high-quality peptides that defined nonoverlapping regions across the protein sequence. Overall, the results indicated that E2c2 in the E2c2/AR2A complex is flexible, with nine of 15 nonoverlapping peptide regions having greater than 50% deuterium exchange by the first time point. E2 peptides with lower deuterium exchange include one peptide within the β-sandwich, which is expected to be relatively stable because it is involved in backbone hydrogen bonds and relatively inaccessible, and five peptide regions within the back layer, which are protected by interaction with Fab AR2A (Fig. 2 *A* and *B* and Fig. S5). The most flexible regions are the front layer of the CD81bs and VR2, with over 90% deuterium exchange for all peptides by the first time point (10 s) (Fig. 2*A*). The variable region 3 (VR3) on E2 is also highly flexible, as expected from its high B-values in the available crystal structures, with 80% deuterium exchange by the first time point compared with 50% deuterium exchange for the peptides covering the β-sandwich. This high global rate of deuterium exchange is comparable to the global deuterium exchange rate of HIV-1 gp120 monomer (38), another viral envelope glycoprotein known to be quite flexible from structural studies (39), and is consistent with the use of flexibility by viral proteins to tolerate mutations (40). To validate our method, we used HDX to map the known bNAb AP33 epitope, which, like the epitope of HCV1, consists of the AS412 with no additional E2 protein components (18, 19) (Fig. S5). As expected, the HDX profile of E2c2-AR2A-AP33 is mostly equivalent to the profile of E2c2-AR2A except with much slower exchange at Asn415-Trp420 within AS412 (Fig. 2*B*).

Next, we sought to extend our HDX studies to the full-length E2ΔTM, which includes hypervariable region 1 (HVR1) and the C-terminal stalk (residues 384–411 and 646–717, respectively), both of which are truncated in E2c2. A previous EM study with E2ΔTM suggested that HVR1 might pack against a highly conserved hydrophobic surface identified on E2c (14). Thus, HVR1 might aid in stabilizing E2 by covering this hydrophobic surface, which, in turn, might stabilize HVR1 through the interaction. The same study also suggested that the C-terminal stalk region might be packed closely against the E2 back layer, further implying that the additional E2 protein regions on E2ΔTM that are absent in E2c2 could have an overall stabilizing effect. However, the HDX results for E2ΔTM in an E2ΔTM/AR2A/AP33 complex were surprisingly comparable to the results for E2c2 described above (Fig. S5). For example, the peptide regions that overlap between E2ΔTM and E2c2 displayed similar levels of

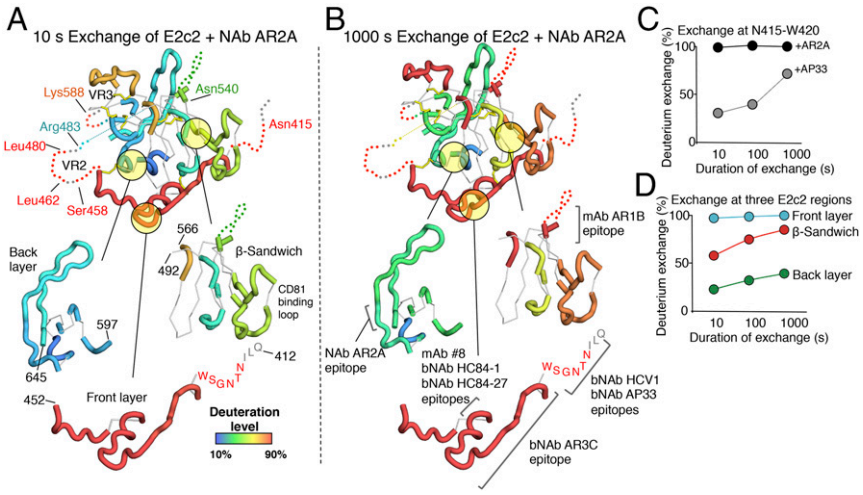

Fig. 2. Structural analysis of HDX data. (*A*, *Top*) Deuterium incorporation into E2c2 when bound to NAb AR2A after 10 s of exchange is mapped onto the crystal structure of E2c using a color gradient. Disordered regions are represented by dotted lines, and regions not covered by peptic fragments and prolines are shown as thin, white tubes if structured or as gray dots if disordered. (*A*, *Bottom*) For clarity, the front layer, the β-sandwich, and the back layer of E2 are displayed individually. (*B*, *Top*) Deuterium exchange into E2c2 bound to NAb AR2A after 1,000 s of exchange is displayed as in *A*. (*B*, *Bottom*) Known mAb epitopes are highlighted. (*C*) HDX of a peptide spanning the N-terminal antigenic region of the CD81bs is plotted for E2c2-AR2A and E2c2-AR2A-AP33. (*D*) Average HDX of the E2 front layer (cyan), β-sandwich (red), and back layer (green) within the E2c2/AR2A complex is plotted.

flexibility, suggesting the HVR1 and the C-terminal stalk did not stabilize the core of the E2 protein. Nevertheless, two peptide fragments from the front layer had less deuterium exchange in E2ΔTM compared with E2c2, although this reduced deuterium exchange was modest and only apparent at the earliest time point (10 s) and more subject to experimental variability (Fig. S5). Lower exchange in the front layer is also shown in a previously published HDX study of fully glycosylated E2ΔTM from a different strain (41). Furthermore, over 90% deuterium exchange was observed for all peptides spanning HVR1 of E2ΔTM by the first time point, suggesting HVR1 is at least as flexible as the front layer and VR2 of E2c2. Thus, in addition to being hypervariable in sequence, HVR1 is highly exposed and likely very heterogeneous in conformation, which could serve to distract the immune response. Finally, the C-terminal stalk region also appeared flexible in our study, with four of seven peptide regions having more than 60% deuterium exchange by the first time point. Although less flexible than the front layer or HVR1, the deuterium exchange profile of the C-terminal stalk is comparable to the long CD81bl extending from the β-sandwich (Gly523–Asp535) in E2c2.

Importantly, our HDX studies revealed that the E2 front layer, which constitutes most of the CD81bs, is remarkably flexible. Although displaying slower deuterium exchange than the front layer, the CD81bl is also relatively flexible compared with other E2 regions. The high flexibility was not notably affected by the presence or absence of HVR1 or the C-terminal stalk. The high flexibility of the front layer is surprising because in the crystal structure, 20% of the front layer consists of a helical region, whose backbone amides should be protected through hydrogen bonding, and because the front layer is stapled to the rest of the E2 protein by two disulfide bonds in a manner that partially buries multiple front layer backbone amides. Nonetheless, this finding now provides a possible explanation of recent structural studies of antibodies that target AS434 on the front layer. Specifically, HC84-27 (23) and weakly neutralizing mAb 8 (24) bind to a peptide spanning AS434 from opposite sides (Fig. S6). When superposed on the E2c-AR3C crystal structure, bNAb HC84-27 does not clash with the E2 protein and binds at an angle of approach comparable to bNAb AR3C, the antibody present in the E2c crystal structure. However, mAb 8 would severely clash with E2 if superposed on the E2c structure in the same manner because its epitope is buried by the E2 β-sandwich (24, 42). The ability of mAb 8 to neutralize some viruses, albeit weakly, suggests that major conformational rearrangements at AS434 are possible that would allow mAb 8 to bind without a clash. Such conformational flexibility of AS434 is now supported by the HDX findings. AS434 rearrangement would entail a nearly 180° rotation of the AS434 helix, and would possibly require disulfide bonds that link the front layer with the rest of the E2 core to adopt alternate, extended disulfide conformations. For example, alternating conformations of a disulfide linking the I-EGF1 and I-EGF2 domains of β2 integrin are able to accommodate a remarkable >20-Å hinge motion between the domains (43, 44). Considering the poor neutralizing ability of mAb 8, the alternative AS434 conformation that is recognized by mAb 8 might not be optimal for vaccine design.

Mapping the Conformational Flexibility of E2 by MD Simulations. The HDX and EM experiments provided empirical evidence for flexibility at the CD81bs of E2. To assess the flexibility of the CD81bs further, we performed MD analysis on unbound E2c from the published E2c-Fab AR3C crystal structure (14) (Fig. S7). The Cα root mean square fluctuation (RMSF) over a 100-ns simulation was used as a measure of the flexibility. Consistent with the HDX study, MD indicated that the front layer was one of the most flexible regions of E2c (Figs. S5 and S7*A*). Within the front layer, regions of high flexibility include residues 420–423, 431–434, and 448–452, each with an average 2.7-Å RMSF (Fig. S7*C*), which is threefold higher than the 0.9-Å RMSF observed for the β-sandwich. Overall, the unliganded E2 front layer appeared to prefer conformations that drift away from the central β-sandwich of the E2 protein, with a 5- to 6-Å RMSD relative to the antibody-bound conformation (Fig. 3*C*). Interestingly, the most populated cluster of conformations adopted by the front layer is characterized by an extended conformation of the AS434 helical region, in which loops extending from the helix deviate 7–8 Å from the bNAb-bound conformation in the crystal structure (Fig. S7). This conformational difference is surprising because the Cys452–Cys620 disulfide bond staples the nearby C terminus of the front layer to the more stable back layer. However, the MD results revealed that this disulfide bond appears to accommodate the conformational differences by potentially adopting alternate orientations (Fig. S7*E*), as previously observed for the integrin subunits discussed above (43, 44). Together with the HDX data, the MD findings further support the conclusion that the front layer is conformationally flexible.

Thermal Stability of HCV E2. The observed high conformational flexibility of recombinant E2 suggests that E2 might be a relatively unstable protein, which could be detrimental for vaccine development. To assess the global thermal stability of E2, we first analyzed E2ΔTM using DSC (Fig. 3*A*). Unexpectedly, the DSC profile of E2ΔTM displayed a single unfolding peak with a high thermal denaturation midpoint (T_m) of 84.8 °C, comparable to the DSC profiles of proteins from thermophilic organisms (45), which generally display T_m values above 80 °C. Furthermore, the E2ΔTM T_m is substantially higher than other viral envelope proteins, such as HIV-1 gp140 (68.1 °C) (46) and influenza hemagglutinin (67.9 °C) (47). However, the DSC unfolding peak of E2ΔTM is relatively broad, with a transition width ($\Delta T_{1/2}$) of 10.6 °C, which is nearly twice the $\Delta T_{1/2}$ of HIV-1 gp140 (46, 48). A broad $\Delta T_{1/2}$ may be indicative of a multistep, noncooperative unfolding transition, suggesting the protein may contain different domains that unfold independently (49, 50). Next, to determine the influence of the C-terminal stalk region and the N-terminal HVR1 on the stability of E2, we analyzed the E2c construct that lacks these components. As suggested by the HDX analysis above, lack of the stalk and HVR1 had only a modest effect on the

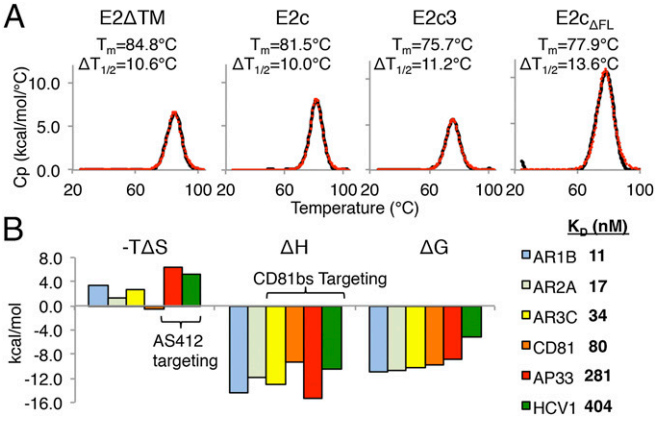

Fig. 3. Calorimetry studies of HCV E2ΔTM. (*A*) DSC denaturation curves for E2ΔTM, E2c, E2c3, and E2c$_{\Delta FL}$ are displayed. The T_m and $\Delta T_{1/2}$ values are indicated next to the curves. The raw data are shown in black, whereas the fitted curves, from which are derived the T_m and $\Delta T_{1/2}$ values, are shown as red dots. (*B*, *Left*) ITC analysis of E2ΔTM binding to AR1B, AR2A, AR3C, CD81, AP33, and HCV1 is presented in a graph. (*B*, *Right*) Binding K_d of each interaction is shown. Values for −TΔS, ΔH, ΔG, and K_d are the averages of results from three ITC experiments. Representative isotherms are illustrated in Fig. S8.

stability of E2c, which has a T_m of 81.5 °C. However, the unfolding peak of E2c remained broad, with a $\Delta T_{1/2}$ of 10.0 °C, indicating that this construct still displayed a noncooperative unfolding behavior.

We next investigated how the flexible, surface-accessible regions that are poorly defined in the electron density in the E2c crystal structure might affect the melting profile of E2. Thus, we modified the E2c construct to E2c3 by truncating loops at residues 569–581 and 585–597, which overlap VR3 and the following disordered region. The removal of these loops from E2c did not affect protein expression and purification, although E2c3 had a lower T_m of 75.7 °C, nearly twice the difference in T_m between E2c and E2ΔTM, but with a similar $\Delta T_{1/2}$ (11.2 °C). This finding indicated that truncation of a flexible and variable region between the β-sandwich and back layer had a destabilizing effect on E2, but did not result in a more cooperative melting curve.

Lastly, to study the contribution of the front layer to the overall thermal stability of E2, we generated an E2c construct lacking the front layer ($E2c_{\Delta FL}$). The $E2c_{\Delta FL}$ had a T_m of 77.9 °C, suggesting it is less stable than E2c, but surprisingly more stable than E2c3. The result implies that E2 thermal stability is more tolerant of a front layer deletion than truncation of the flexible VR3 region defined previously (14). A recent crystal structure of $E2c_{\Delta FL}$ from a genotype 2a HCV further supports a relatively minimal role of the E2 front layer in overall E2 stability (41). Thus, despite the flanking disulfide bridges to the β-sandwich and back layer, the front layer might be more akin to a flexible loop than a rigid structural element stably integrated with the rest of the E2 protein.

Thermodynamic Parameters of HCV E2 Interactions with Ligands. The change in entropy during protein binding, −TΔS, can be an indication of structural ordering induced by ligand binding. For example, with interactions between HIV-1 gp120 monomer and CD4 (and similar ligands), high and unfavorable −TΔS correlates with the induction of structural rearrangement (51). Here, we used ITC to measure the −TΔS of binding to HCV E2ΔTM by the CD81bs-targeting ligands bNAbs AR3C, AP33, and HCV1 and by the large external loop of CD81 (Fig. 3*B* and Fig. S8). For comparison, we also measured binding to E2ΔTM by a non-CD81bs–directed ligand mAb, AR1B.

The ITC results indicated that all ligands tested bound tightly to E2ΔTM. The −TΔS of the CD81bs-targeting AR3C (2.79 kcal/mol) and CD81 (−0.44 kcal/mol) was modest. However, the −TΔS of AR3C and CD81 did not notably differ from the −TΔS of the non–CD81bs-directed antibodies AR2A (1.25 kcal/mol) and AR1B (3.43 kcal/mol). By contrast, the −TΔS of AS412 targeting bNAbs AP33 (6.26 kcal/mol) and HCV1 (5.44 kcal/mol) was nearly twofold higher than for AR3C, suggesting more stabilization on binding to the 12-residue AS412 than the other CD81bs components. In comparison to the high −TΔS observed for CD4 binding to gp120 (55 kcal/mol) (51), it appears that CD81bs recognition does not entail large, global conformational changes in E2.

Conclusion

Our investigations of E2 antigens by EM, HDX, and MD have shown that the CD81bs exhibits high structural flexibility. Our results extend and confirm previous observations and speculations made from crystal structures showing that the AS412 region is disordered when unbound (14, 41) and adopts a hairpin or open-loop conformation when complexed with different NAbs (17–22). Such alternate conformations appear to be critical for virus neutralization. A recent study by Sandomenico et al. (52) showed that antibodies raised against cyclized AS412 peptides that adopt an alternative conformation were not neutralizing. From the present study, the CD81bs front layer resembles a highly flexible loop despite being held by two disulfide bonds and despite high sequence conservation, which is generally not associated with flexible loops in viral proteins. High flexibility is consistent with the observation that soluble E2 and E1E2 can elicit antibodies that can bind the CD81bs with high affinity but, nonetheless, cannot neutralize the virus (27–31). Some of these non-NAbs or weak NAbs could be similar to mAb 8, which recognizes a conformation likely to be poorly accessible on the virus (Fig. S6). By mapping E2 conformational dynamics, the data here provide a molecular explanation for why it is difficult to elicit CD81bs NAbs to the virus using recombinant E2. In contrast to HIV, which has a recessed CD4 receptor-binding site, the CD81bs on HCV is fully accessible (Fig. S1), and yet NAbs to CD81bs are difficult to elicit because of conformational flexibility. Interestingly, the DSC findings indicated that although E2 is flexible, it is also thermally stable, at least in its core region, presumably due to its high density of disulfide bonds. It appears that in E2, HCV has evolved a highly stable β-sandwich scaffold stabilized by conserved disulfide bonds to accommodate both sequence variation and conformational flexibility. Of note, the observations made with the soluble E2 antigens may differ in the context of E2 on the viral surface. Nonetheless, next-generation soluble E2 antigens with a more stabilized CD81bs that is in a functional conformation recognized by NAbs may now be engineered based on these E2 flexibility results and published structures. Indeed, antigen stabilization as a rational vaccine design strategy to enhance NAb production has been demonstrated for respiratory syncytial virus (53), and is being actively pursued for HIV (54, 55). Further work in determining E2 CD81bs flexibility on the E1E2 complex and the virion is warranted to improve immunogen design targeting this important conserved functional site on HCV.

Materials and Methods

Antibodies. Fabs were either generated from papain (Sigma) digestion of the corresponding IgGs or expressed in *Escherichia coli* (BL21 strain; Novagen) as described previously (14).

E2 Proteins. The four soluble E2 constructs in this study were E2ΔTM, E2c2, E2c3, and $E2c_{\Delta FL}$ (Fig. S2). The constructs were produced in 293F cells in the presence of kifunesine.

HDX. Protein complexes analyzed by HDX were introduced to an Orbitrap Elite Mass Spectrometer (ThermoFisher Scientific) for electrospray ionization and accurate mass measurements. DXMS Explorer (Sierra Analytics) was used for the calculation of the deuteration level of all of the peptides as described previously (56, 57).

ITC. ITC binding experiments were performed using a MicroCal Auto-iTC200 instrument (GE Healthcare).

DSC. Thermal melting curves of fully glycosylated HCV E2 glycoproteins were obtained with a MicroCal VP-Capillary calorimeter (Malvern).

EM. Size exclusion chromatography-purified, EndoH-treated E2/Fab complexes were imaged on an FEI Tecnai F20 instrument at 200 kV transmission electron microscope (TEM) equipped with a Gatan Ultrascan 4k × 4k CCD. Data were collected using Leginon Multi-Scale Imaging and processed with TiltPicker (58), Xmipp (59), SPIDER (60), and EMAN1 (61).

MD Simulations. MD simulations were performed using the Desmond MD package with the Maestro–Desmond interoperability tool, version 2.0 (62).

Further details of materials and methods used in this study are provided in *SI Materials and Methods*.

ACKNOWLEDGMENTS. R.U.K. thanks the Swiss National Science Foundation for a postdoctoral fellowship. This work is supported by NIH Grants AI079031 and AI123861 (to M.L.); NIH Grants AI106005 and AI123365 (to M.L. and I.A.W.); NIH Grant GM094586 (to I.A.W.); and NIH Grants AI117905, GM020501, and AI101436 (to S.L.), as well as the Skaggs Institute (I.A.W.). This article is manuscript 29353 from The Scripps Research Institute.

1. Messina JP, et al. (2015) Global distribution and prevalence of hepatitis C virus genotypes. *Hepatology* 61(1):77–87.
2. Thursz M, Fontanet A (2014) HCV transmission in industrialized countries and resource-constrained areas. *Nat Rev Gastroenterol Hepatol* 11(1):28–35.
3. Feeney ER, Chung RT (2014) Antiviral treatment of hepatitis C. *BMJ* 348:g3308.
4. Pawlotsky JM, Feld JJ, Zeuzem S, Hoofnagle JH (2015) From non-A, non-B hepatitis to hepatitis C virus cure. *J Hepatol* 62(1, Suppl):S87–S99.
5. Zhang Z, et al. (2013) Hepatitis C virus genotype diversity among intravenous drug users in Yunnan Province, Southwestern China. *PLoS One* 8(12):e82598.
6. Ly KN, et al. (2012) The increasing burden of mortality from viral hepatitis in the United States between 1999 and 2007. *Ann Intern Med* 156(4):271–278.
7. Marco A, et al. (2013) Hepatitis C virus reinfection among prisoners with sustained virological response after treatment for chronic hepatitis C. *J Hepatol* 59(1):45–51.
8. Midgard H, et al. (2016) Hepatitis C reinfection after sustained virological response. *J Hepatol* 64(5):1020–1026.
9. Kong L, Jackson KN, Wilson IA, Law M (2015) Capitalizing on knowledge of hepatitis C virus neutralizing epitopes for rational vaccine design. *Curr Opin Virol* 11:148–157.
10. Walker CM, Grakoui A (2015) Hepatitis C virus: Why do we need a vaccine to prevent a curable persistent infection? *Curr Opin Immunol* 35:137–143.
11. Cox AL (2015) MEDICINE. Global control of hepatitis C virus. *Science* 349(6250): 790–791.
12. Zona L, et al. (2014) CD81-receptor associations–impact for hepatitis C virus entry and antiviral therapies. *Viruses* 6(2):875–892.
13. Douam F, Lavillette D, Cosset FL (2015) The mechanism of HCV entry into host cells. *Prog Mol Biol Transl Sci* 129:63–107.
14. Kong L, et al. (2013) Hepatitis C virus E2 envelope glycoprotein core structure. *Science* 342(6162):1090–1094.
15. Owsianka AM, et al. (2006) Identification of conserved residues in the E2 envelope glycoprotein of the hepatitis C virus that are critical for CD81 binding. *J Virol* 80(17): 8695–8704.
16. Drummer HE, Wilson KA, Poumbourios P (2002) Identification of the hepatitis C virus E2 glycoprotein binding site on the large extracellular loop of CD81. *J Virol* 76(21): 11143–11147.
17. Kong L, et al. (2012) Structure of hepatitis C virus envelope glycoprotein E2 antigenic site 412 to 423 in complex with antibody AP33. *J Virol* 86(23):13085–13088.
18. Kong L, et al. (2012) Structural basis of hepatitis C virus neutralization by broadly neutralizing antibody HCV1. *Proc Natl Acad Sci USA* 109(24):9499–9504.
19. Potter JA, et al. (2012) Toward a hepatitis C virus vaccine: The structural basis of hepatitis C virus neutralization by AP33, a broadly neutralizing antibody. *J Virol* 86(23):12923–12932.
20. Pantua H, et al. (2013) Glycan shifting on hepatitis C virus (HCV) E2 glycoprotein is a mechanism for escape from broadly neutralizing antibodies. *J Mol Biol* 425(11): 1899–1914.
21. Meola A, et al. (2015) Structural flexibility of a conserved antigenic region in hepatitis C virus glycoprotein E2 recognized by broadly neutralizing antibodies. *J Virol* 89(4): 2170–2181.
22. Li Y, et al. (2015) Structural basis for penetration of the glycan shield of hepatitis C virus E2 glycoprotein by a broadly neutralizing human antibody. *J Biol Chem* 290(16): 10117–10125.
23. Krey T, et al. (2013) Structural basis of HCV neutralization by human monoclonal antibodies resistant to viral neutralization escape. *PLoS Pathog* 9(5):e1003364.
24. Deng L, et al. (2013) Structural evidence for a bifurcated mode of action in the antibody-mediated neutralization of hepatitis C virus. *Proc Natl Acad Sci USA* 110(18): 7418–7422.
25. Law M, et al. (2008) Broadly neutralizing antibodies protect against hepatitis C virus quasispecies challenge. *Nat Med* 14(1):25–27.
26. Giang E, et al. (2012) Human broadly neutralizing antibodies to the envelope glycoprotein complex of hepatitis C virus. *Proc Natl Acad Sci USA* 109(16):6205–6210.
27. Ray R, et al. (2010) Characterization of antibodies induced by vaccination with hepatitis C virus envelope glycoproteins. *J Infect Dis* 202(6):862–866.
28. Meyer K, Banerjee A, Frey SE, Belshe RB, Ray R (2011) A weak neutralizing antibody response to hepatitis C virus envelope glycoprotein enhances virus infection. *PLoS One* 6(8):e23699.
29. Zhang P, et al. (2007) Hepatitis C virus epitope-specific neutralizing antibodies in Igs prepared from human plasma. *Proc Natl Acad Sci USA* 104(20):8449–8454.
30. Ruwona TB, Giang E, Nieusma T, Law M (2014) Fine mapping of murine antibody responses to immunization with a novel soluble form of hepatitis C virus envelope glycoprotein complex. *J Virol* 88(18):10459–10471.
31. Ball JK, Tarr AW, McKeating JA (2014) The past, present and future of neutralizing antibodies for hepatitis C virus. *Antiviral Res* 105:100–111.
32. Wellnitz S, et al. (2002) Binding of hepatitis C virus-like particles derived from infectious clone H77C to defined human cell lines. *J Virol* 76(3):1181–1193.
33. Triyatni M, et al. (2002) Structural features of envelope proteins on hepatitis C virus-like particles as determined by anti-envelope monoclonal antibodies and CD81 binding. *Virology* 298(1):124–132.
34. McLellan JS, et al. (2011) Structure of HIV-1 gp120 V1/V2 domain with broadly neutralizing antibody PG9. *Nature* 480(7377):336–343.
35. Englander SW (2006) Hydrogen exchange and mass spectrometry: A historical perspective. *J Am Soc Mass Spectrom* 17(11):1481–1489.
36. Konermann L, Pan J, Liu YH (2011) Hydrogen exchange mass spectrometry for studying protein structure and dynamics. *Chem Soc Rev* 40(3):1224–1234.
37. Bale S, et al. (2011) Ebola virus glycoprotein needs an additional trigger, beyond proteolytic priming for membrane fusion. *PLoS Negl Trop Dis* 5(11):e1395.
38. Kong L, et al. (2010) Local conformational stability of HIV-1 gp120 in unliganded and CD4-bound states as defined by amide hydrogen/deuterium exchange. *J Virol* 84(19): 10311–10321.
39. Chen L, et al. (2009) Structural basis of immune evasion at the site of CD4 attachment on HIV-1 gp120. *Science* 326(5956):1123–1127.
40. Tokuriki N, Oldfield CJ, Uversky VN, Berezovsky IN, Tawfik DS (2009) Do viral proteins possess unique biophysical features? *Trends Biochem Sci* 34(2):53–59.
41. Khan AG, et al. (2014) Structure of the core ectodomain of the hepatitis C virus envelope glycoprotein 2. *Nature* 509(7500):381–384.
42. Deng L, et al. (2014) Discrete conformations of epitope II on the hepatitis C virus E2 protein for antibody-mediated neutralization and nonneutralization. *Proc Natl Acad Sci USA* 111(29):10690–10695.
43. Shi M, et al. (2007) A structural hypothesis for the transition between bent and extended conformations of the leukocyte β2 integrins. *J Biol Chem* 282(41): 30198–30206.
44. Smagghe BJ, Huang PS, Ban YE, Baker D, Springer TA (2010) Modulation of integrin activation by an entropic spring in the β-knee. *J Biol Chem* 285(43):32954–32966.
45. Razvi A, Scholtz JM (2006) Lessons in stability from thermophilic proteins. *Protein Sci* 15(7):1569–1578.
46. Sanders RW, et al. (2013) A next-generation cleaved, soluble HIV-1 Env trimer, BG505 SOSIP.664 gp140, expresses multiple epitopes for broadly neutralizing but not non-neutralizing antibodies. *PLoS Pathog* 9(9):e1003618.
47. Epand RM, Epand RF (2002) Thermal denaturation of influenza virus and its relationship to membrane fusion. *Biochem J* 365(Pt 3):841–848.
48. Brower ET, Schön A, Freire E (2010) Naturally occurring variability in the envelope glycoprotein of HIV-1 and development of cell entry inhibitors. *Biochemistry* 49(11): 2359–2367.
49. Morar-Mitrica S, Nesta D, Crotts G (2013) Differential scanning calorimetry (DSC) for biopharmaceutical development: Old concepts, new applications. *Biopharma Asia* 2(4):44–55.
50. Deller MC, Kong L, Rupp B (2016) Protein stability: A crystallographer's perspective. *Acta Crystallogr F Struct Biol Commun* 72(Pt 2):72–95.
51. Myszka DG, et al. (2000) Energetics of the HIV gp120-CD4 binding reaction. *Proc Natl Acad Sci USA* 97(16):9026–9031.
52. Sandomenico A, et al. (2016) Generation and characterization of monoclonal antibodies against a cyclic variant of hepatitis C virus E2 epitope 412-422. *J Virol* 90(7): 3745–3759.
53. McLellan JS, et al. (2013) Structure-based design of a fusion glycoprotein vaccine for respiratory syncytial virus. *Science* 342(6158):592–598.
54. Guenaga J, et al. (2015) Well-ordered trimeric HIV-1 subtype B and C soluble spike mimetics generated by negative selection display native-like properties. *PLoS Pathog* 11(1):e1004570.
55. Kong L, et al. (2016) Uncleaved prefusion-optimized gp140 trimers derived from analysis of HIV-1 envelope metastability. *Nat Commun* 7:12040.
56. Mendillo ML, et al. (2009) A conserved MutS homolog connector domain interface interacts with MutL homologs. *Proc Natl Acad Sci USA* 106(52):22223–22228.
57. Chen H, et al. (2010) Allosteric inhibition of complement function by a staphylococcal immune evasion protein. *Proc Natl Acad Sci USA* 107(41):17621–17626.
58. Voss NR, Yoshioka CK, Radermacher M, Potter CS, Carragher B (2009) DoG Picker and TiltPicker: Software tools to facilitate particle selection in single particle electron microscopy. *J Struct Biol* 166(2):205–213.
59. Scheres SH, et al. (2005) Maximum-likelihood multi-reference refinement for electron microscopy images. *J Mol Biol* 348(1):139–149.
60. Frank J, et al. (1996) SPIDER and WEB: Processing and visualization of images in 3D electron microscopy and related fields. *J Struct Biol* 116(1):190–199.
61. Ludtke SJ, Baldwin PR, Chiu W (1999) EMAN: Semiautomated software for high-resolution single-particle reconstructions. *J Struct Biol* 128(1):82–97.
62. Bowers KJ, et al. (2006) Scalable algorithms for molecular dynamics simulations on commodity clusters. *Proceedings of the 2006 ACM/IEEE Conference on Supercomputing* (*SC06*) (ACM Press, New York).
63. Erntell M, Myhre EB, Sjöbring U, Björck L (1988) Streptococcal protein G has affinity for both Fab- and Fc-fragments of human IgG. *Mol Immunol* 25(2):121–126.
64. Hastie KM, et al. (2011) Crystal structure of the Lassa virus nucleoprotein-RNA complex reveals a gating mechanism for RNA binding. *Proc Natl Acad Sci USA* 108(48): 19365–19370.
65. Marsh JJ, et al. (2013) Structural insights into fibrinogen dynamics using amide hydrogen/deuterium exchange mass spectrometry. *Biochemistry* 52(32):5491–5502.
66. Suloway C, et al. (2005) Automated molecular microscopy: The new Leginon system. *J Struct Biol* 151(1):41–60.
67. Jorgensen WL, Maxwell DS, TiradoRives J (1996) Development and testing of the OPLS all-atom force field on conformational energetics and properties of organic liquids. *J Am Chem Soc* 118:11225–11236.
68. Krautler V, van Gunsteren WF, Hunenberger PH (2001) A fast SHAKE: Algorithm to solve distance constraint equations for small molecules in molecular dynamics simulations. *J Comput Chem* 22:501–508.
69. Martyna GJ, Tobias DJ, Klein ML (1994) Constant-pressure molecular-dynamics algorithms. *J Chem Phys* 101:4177–4189.
70. Hoover WG (1985) Canonical dynamics: Equilibrium phase-space distributions. *Phys Rev A Gen Phys* 31(3):1695–1697.
71. Darden TA, York DM, Pedersen LG (1993) Particle mesh Ewald: An N·log(N) method for Ewald sums in large systems. *J Chem Phys* 98:10089–10092.
72. Tuckerman M, Berne BJ, Martyna GJ (1992) Reversible multiple time scale molecular-dynamics. *J Chem Phys* 97:1990–2001.